Sensitivity and dynamic phase response
to thermal radiation
of a polarization-maintaining fiber

Martin KYSELAK[1*], Filip DVORAK[2], Jan MASCHKE[1], Cestmir VLCEK[1]

[1]Department of Electrical Engineering, Faculty of Military Technology, University of Defence,
 Kounicova 65, Brno, Czech Republic

[2]Department of Radar Technology, Faculty of Military Technology, University of Defence,
 Kounicova 65, Brno, Czech Republic

*Corresponding author: martin.kyselak@unob.cz

This paper deals with the phase shift development between two polarization modes in birefringent fiber, caused by body heat transfer of different temperatures. The aim is to analyze sensitivity and dynamic behaviors, which are significant when optical fiber is used as a sensor of temperature field disturbance. The analysis is based on the values measured during thermal exposure of a section of type PANDA birefringent optical fiber to heat emitted by an exposure body of chosen temperature, placed at a defined distance. The effect of heat transfer through conduction and convection is suppressed by shielding with plastic wraps. The analyzed results, the Stokes parameters and subsequent phase shift, are measured by the polarimeter. The paper follows up on previously published measurement results.

Keywords: fiber sensor, polarization-maintaining fiber (PMF), optical fiber, birefringence, temperature field disturbance, approximation equations, approximation parameters.

1. Introduction

The proposed sensor of temperature field disturbance is based on the highly birefringent optical fiber, where both polarization axes are identically excited. As an effect of outer thermal energy and subsequent temperature change of the fiber, the velocity of propagating polarization modes is changed, with a subsequent phase shift between them.

Optical fiber response was verified for different thermal exposure and optical fiber pattern arrangements, various exposed lengths and different optical fiber wavelengths. Experiments showed a large phase response to surrounding, often undesirable, thermal influences. The results were published on a continuous basis [1–5].

Because of the problematically defined heat transfer via radiation, conduction and convection, a specific arrangement was chosen. The exposed section of the fiber was

placed in a shielded foil space. This resulted in limiting the influence of heat by conduction and convection.

When constructing the sensor itself, the same polarization modes excitation is expected, and the output polarization state is evaluated using a polarizer rotated by an angle of π/4 to polarization axes [6, 7]. In the experimental arrangement, this requirement was satisfied by introducing linearly polarized radiation at an angle of π/4 to the polarization axes. The output was measured by a polarimeter, allowing the measurement of the Stokes parameters, the polarization degrees and the resulting phase shift. Suppression of environmental impact was achieved via secondary protection of optical fibers in unexposed segments.

The measurement site and a set of measurement results were published in [1]. The introductory sections summarize some data about the workplace layout and measurement results. The main attention is paid to the analysis of acquired results and descriptions through sensitivity and dynamic characteristics.

A similar measurement of the dependence of the change in the polarization state on the high birefringence optical fibers is dealt with in other research works [8–11].

2. Principle of sensor arrangement

To achieve maximal sensor sensitivity, it is necessary to excite identically the two polarization modes of the fiber characterized by different refractive indexes. This condition can be fulfilled via circular polarization or by rotating the linear polarized light by π/4 with respect to the polarization axes.

A disadvantage of the first possibility is the necessity of using a quarter-wave plate, which is difficult in the case of fiber arrangement [12]. Much better is the second method with identical excitation of both polarization planes provided by mutually rotating the source pigtail and the sensor fiber by an angle of π/4. This arrangement can be im-
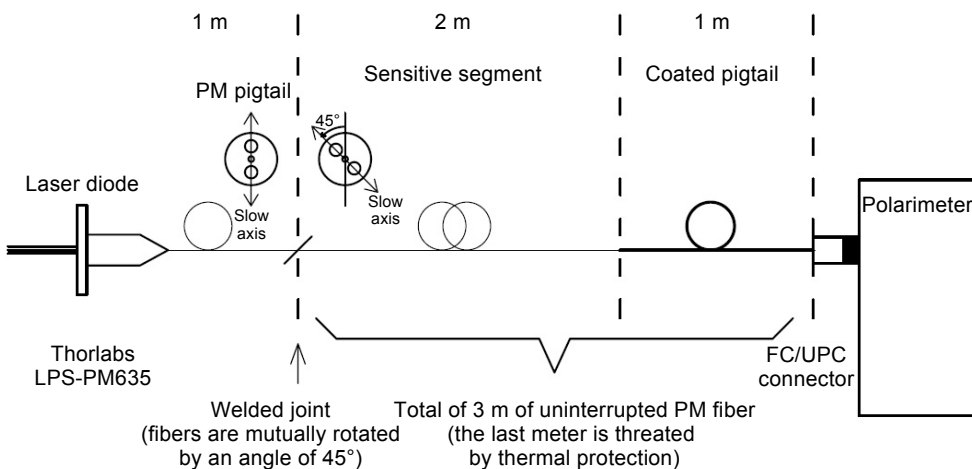
Fig. 1. Schematic arrangement for measurement of sensor fiber response.

plemented by means of oriented fiber fixation in the connector or by a splice with the same fiber orientation. Both variants are available in the laboratory but in the following text, only the splice variant prepared by SQS Company is studied. A schematic arrangement for the measurement of sensor fiber response is given in Fig. 1.

The analytical description assumes an ideal state where we do not consider inaccuracies in the mutual adjustment of the angles of the optical fibers and the influence of bending and twisting, which is negligible in relation to the geometry of the arrangement, *etc*. Likewise, the final coherence with regard to the bandwidth of the sources used is not considered.

At the fiber output, the Stokes parameters are measured by the polarimeter [1]

$$S_0 = E^2, \quad S_1 = 0, \quad S_2 = -E^2\cos(\delta), \quad S_3 = -E^2\sin(\delta) \tag{1}$$

The corresponding phase shift is

$$\delta = \arctan\left(\frac{S_3}{S_2}\right) \tag{2}$$

3. Measuring conditions and organization of measuring workplace

The heat transfer mechanism has three basic components: transmission through conduction, convection and radiation. The mechanisms are described in more detail in [1]. In an attempt to define the experimental conditions, two heat transfer mechanisms of conduction and convection were suppressed by the appropriate experimental arrangement, by enclosing the exposed portion of the fiber in a foil cover. The main way of heat transfer thus remains the radiation.

The arrangement of the experimental workplace is shown in Fig. 2. The temperature source is represented by a plastic container with water. This layout allows selecting a higher or lower water temperature in comparison with ambient temperature, and it also allows adjusting different temperature steps. The water container is placed on polystyrene spacers and the polystyrene cover of the measuring workplace. Inserted between the temperature source and the optical fiber sensor is a three-layer plastic wrap to suppress heat conduction and heat convection. To exclude any effect of outer disturbing sources and to prevent heat leakage, a polyethylene film is applied to the complete workplace as a delimiting cover. The water container exchanges heat with two lengths of optical fiber, which lie on a polystyrene board. From the three heat transfer mechanisms, thermal radiation is of the main impact in this arrangement.

The light source was the laser diode LPS-PM635-FC (Thorlabs) mounted in a power supply controller LED driver DC2200 (Thorlabs). The optical power was concentrated into the pigtail of the optical fiber PM630-HP PANDA style. Linear vertical polarized (LVP) light was led into the sensor fiber via the splice. The angle of polarization axes was oriented 45° towards the LVP light (Fig. 1). The length of the optical fiber sensor part was 2 m and the sensor part was without secondary protection.
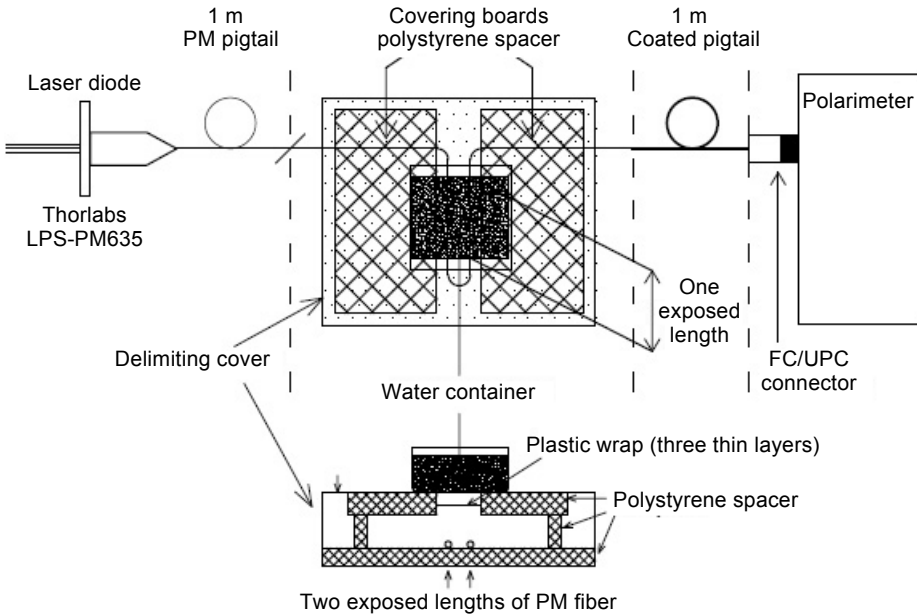
Fig. 2. Floor projection of measuring workplace with exposed length depiction and its sectional view.

The mutual angular rotation of polarization axes invoked almost the same excitation of both the slow axis and the fast axis of the optical fiber sensor part. The total length of exposed optical fiber sensor part was 54 cm. The output optical fiber was 1 m long and was coated with secondary protection to eliminate temperature effects and other outer disturbances. An FC/UPC connector terminated the optical fiber path and was inserted into the polarimeter PAN5710VIS Sensor Head (Thorlabs).

By applying the container with water, the excitation of exposed optical fiber length was initiated. The range of applied temperatures was from 0 to 48°C, the temperature step was 8°C and ambient temperature was 24°C. The temperature source was applied at a time that we mark as the measurement beginning. The distance of the temperature source from the optical fiber sensor was defined by the polystyrene spacer height and covering board thickness. Its value was 9 cm and the space between the covering boards was 12 cm. To limit the influence of convection, the sensor was wrapped in three layers of plastic foil.

4. Experimental results

The results of the measurements are the time courses of the Stokes parameters, the degree of polarization and the resulting phase shift. From the point of view of assumed application, *i.e.* utilization in the temperature field disturbance sensor, the fundamental result is the phase shift waveform.

We are concerned here with periodic waveforms with a rising period corresponding to the process of radiation heating of the fiber. The temperature source is attached at

140 s, which is sufficient to capture the steady state before the fiber is excited and re-moved at 470 s, although there is still no complete stabilization at this time. The measurement time is 330 s. For the sake of completeness, the phase shift is monitored after removal of the heat source.

The measurements were performed for exposure body temperatures of 0, 8, 16, 24, 32, 40 and 48°C. Figures 3 and 4 show the phase shift changes over time for temper-
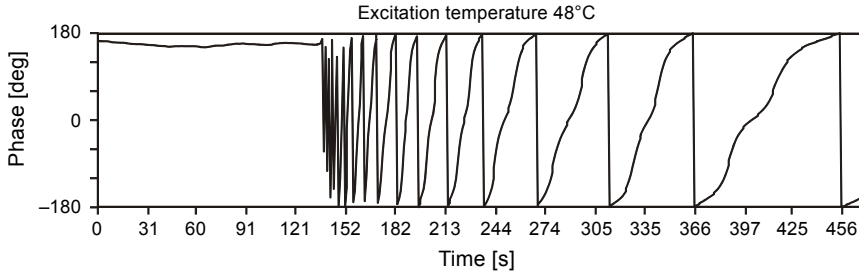
Fig. 3. The phase shift changes over time at 48°C.
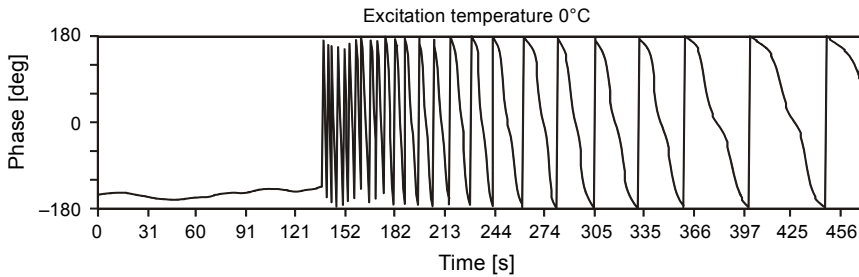
Fig. 4. The phase shift changes over time at 0°C.
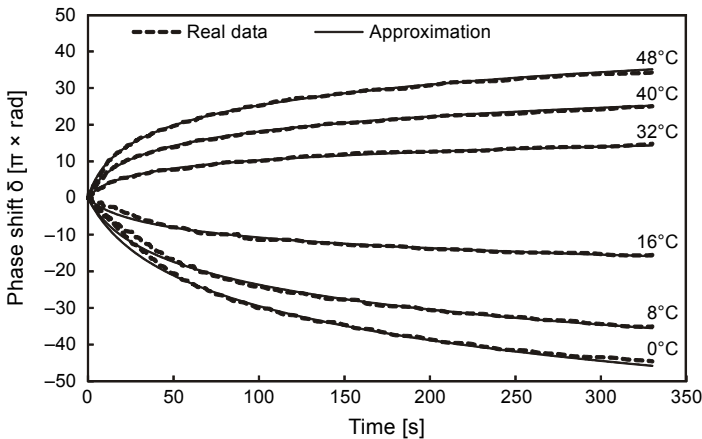
Fig. 5. The phase shift changes over time for temperatures from 0 to 48°C. Phase shift time dependence after correcting for 24°C and complementing approximated waveforms according to relation (7).

atures of 48 and 0°C for a further phase shift analysis. The results will be used to ana-
lyze measurement errors.

Based on the phase changes corresponding to the exposure temperatures, the result-
ing waveform, published in [1], was obtained. The dependence of the resulting phase
shift on temperature is shown in Fig. 5. To exclude the effect of the actual exposure
body on the resulting response, the dependence of the final phase was measured when
the exposure body was applied at ambient temperature. The phase shift measured for
the ambient temperature was subtracted from the phase curves for the other tempera-
tures. The resulting phase curves after the correction are shown in Fig. 5 and are the
subject of further analysis.

5. Analysis of phase shift dependence on exposure temperatures

It follows from the phase waveforms presented in Figs. 3 and 4 that the signal is ape-
riodic in view of the phase shift change. To derive the resulting phase shift time de-
pendence, the following general consideration can be taken into account. The average
velocity of phase shift change $(d\delta/dt)_a$ for a particular period T, *e.g.* the period of the
waveform passing between two zero levels, with the change equal to 2π, is approxi-
mately

$$\left(\frac{d\delta}{dt}\right)_a = \frac{2\pi}{T} \tag{3}$$

The period T is assumed to change linearly in dependence on time, *i.e.*,

$$T = k\xi + \eta \tag{4}$$

After substitution into (3), the relation for average velocity of phase change is obtained

$$\left(\frac{d\delta}{dt}\right)_a = \frac{2\pi}{k\xi + \eta} \tag{5}$$

Actually, it is an angular velocity of phase change in accordance with relation (3).
The general phase development is obtained by integration of relation (5):

$$\delta_a(t) = \int_0^t \frac{2\pi}{k\xi + \eta} d\xi \tag{6}$$

For $\delta_a(t)$, the following equation holds

$$\delta_a(t) = \frac{2\pi}{k} \ln\left(\frac{k}{\eta}t + 1\right) = \pi A \ln\left(\frac{t}{B} + 1\right) \tag{7}$$

where parameters A and B are

$$A = 2/k, \quad B = \eta/k \tag{8}$$

The value π is factored out in view of the measured phase shift being given in multiples of π.

The waveforms of phase shift time dependence for different temperatures in approximation data in Fig. 5 are reduced by subtraction of the 24°C phase shift waveform in comparison with real data in the same picture. At the same time, waveforms corresponding to Eq. (7) are plotted, which are referred to as approximated waveforms. For particular temperatures of the exciting body, the values of parameters A and B are determined using relation (7). It follows from the approximation relations that the assumption of time linear change of the phase shift for particular exposure body temperatures was correct. This is obviously the result of suppressing undesirable heat transfer mechanisms except the desirable thermal radiation.

Approximation equations and the corresponding approximation parameters A and B are presented in the Table. The suitability of approximation partially results from the waveforms presented in Fig. 5. For a more precise evaluation, the relative approximation errors are given below to allow comparison with measured results.

T a b l e. Approximation equations and approximation parameters.

Exposure temperatures	$A = 1/k$	$B = \eta/k$	Approximation functions $\delta_{ap} = A\ln(t/B + 1)$	Normalized approximation functions $\delta_n = \ln(t/B + 1)$
0	−14.9	16	$\delta_{ap}(0) = -14.9\ln(t/16 + 1)$	$\delta_n(0) = \ln(t/16 + 1)$
8	−10.6	12	$\delta_{ap}(8) = -10.6\ln(t/12 + 1)$	$\delta_n(8) = \ln(t/12 + 1)$
16	−4.5	10	$\delta_{ap}(16) = -4.5\ln(t/10 + 1)$	$\delta_n(16) = \ln(t/10 + 1)$
32	3.5	5.6	$\delta_{ap}(32) = 3.5\ln(t/5.6 + 1)$	$\delta_n(32) = \ln(t/5.6 + 1)$
40	6.1	5.4	$\delta_{ap}(40) = 6.1\ln(t/5.4 + 1)$	$\delta_n(40) = \ln(t/5.4 + 1)$
48	8.5	5.4	$\delta_{ap}(48) = 8.5\ln(t/5.4 + 1)$	$\delta_n(48) = \ln(t/5.4 + 1)$

To enhance the suitability of selected approximations, the relative approximation errors are analyzed that are determined by the relation

$$\Delta = \frac{\delta_m - \delta_{ap}}{\delta_m} \tag{9}$$

where Δ is the relative error, δ_m is the measured value of phase shift, and δ_{ap} is the value of approximation.

Waveform approximations for higher than ambient temperatures are analyzed in the first part. The time range is divided into two time intervals, the first interval from 0 to 10 s and the second interval from 10 to 330 s. In the first interval, the approximation follows the measured data almost identically. For the first interval, the relative approximation error waveforms are presented in Fig. 6. The relative errors do not exceed units of percentage points and, obviously, the approximations are suitable and can be applied.

The situation of analysis is different in the second part with the interval from 0 to 10 s. For relative errors computed by relation (9), the values are about tens of per-
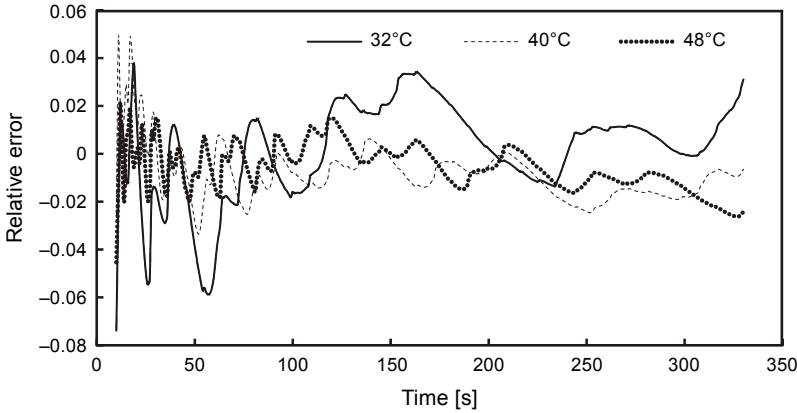
Fig. 6. Approximation relative errors *Δ* for temperatures of 32, 40 and 48°C.

centage points. However, from visual evaluation of the waveforms in Fig. 5 it follows that even here the selected approximation should be satisfactory. Differences between approximated and measured waveforms are mainly introduced by measuring errors. It is obvious from Fig. 3 that the velocity of phase change is higher than the sampling rate of the polarimeter. At the beginning of measuring the waveforms, the range of phase shift is not ±π but less. The approximated waveforms have their origin in the physical model and thus these waveforms depict the phase shift development of a real phenomenon more precisely than the measured waveforms and the approximated waveforms can be taken into account within the analysis process.

Higher inaccuracy occurs in waveforms with exposure temperatures lower than 24°C ambient temperature. Up to the time 50 s, the approximated functions diverge from the measured values, as can be seen in Fig. 5. Relative errors for the time range up to 20 s
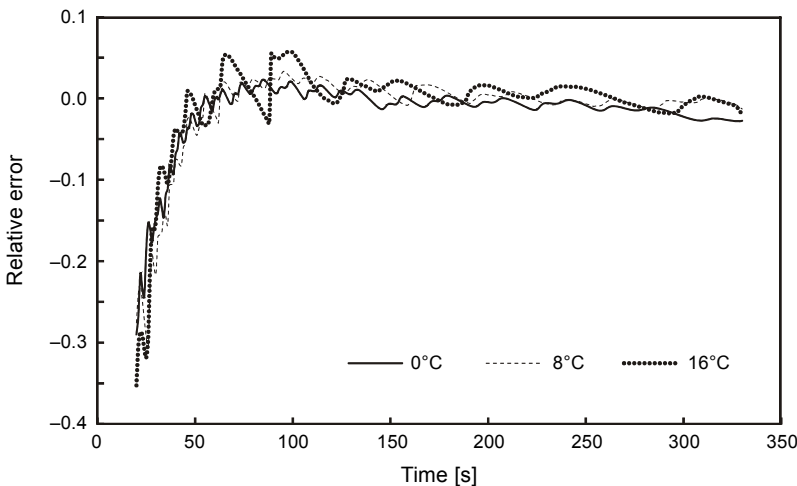
Fig. 7. Approximation relative errors *Δ* for temperatures 0, 8 and 16°C, interval from 20 to 330 s.

are presented in Fig. 7. A major reason for these divergences again consists in the lower polarimeter-sampling rate in comparison with the higher phase shift velocity of a real phenomenon. This is obvious from Fig. 4, where the velocity of phase change within *ca.* 35 s from the beginning of excitation does not achieve values of $\pm\pi$. It can again be admitted that the approximation curve better captures the actual change in phase than the measured values do.

It can be concluded from the error analysis that the approximations fully agree with the measured values and can be applied to the description of fiber phase response in fiber absorption caused by thermal radiation.

Approximation error for the time interval from the exposure beginning 0 to 50 s, except the reasons mentioned above, is also determined by different measuring arrangement. Heat transfer is from the fiber as a body of smaller weight to the exposure body of greater weight. The total fiber response for lower temperatures is greater for times above 50 s in comparison with higher temperatures but, contrary to this, the phase shift velocity is slower for lower temperatures at the exposure beginning.

Approximation equations and normalized approximation equations including logarithmic functions without the parameter *A* are presented in the Table and their waveforms are presented in Fig. 8.

From the parameters of normalized equations and waveforms presented in Fig. 8 it is evident that these waveforms are almost identical for the range of exposure temperatures from 32 to 48°C. This means that the phase change depends on the parameter *A* alone, which can be referred to as sensitivity.

Normalized approximation waveforms have a different development for exposure temperatures of 0, 8 and 16°C (see Fig. 8). The reason for this can be found in a different "heat source–optical fiber" arrangement, where the optical fiber is actually a source of thermal radiation. The other reason can be seen in the layout itself of the water container, where the particular thermal gradient appears on its bottom. It is a state when the temperature of the outside wall of this plastic water container can differ from the temperature of water inside the container. The steepness of normalized waveforms is
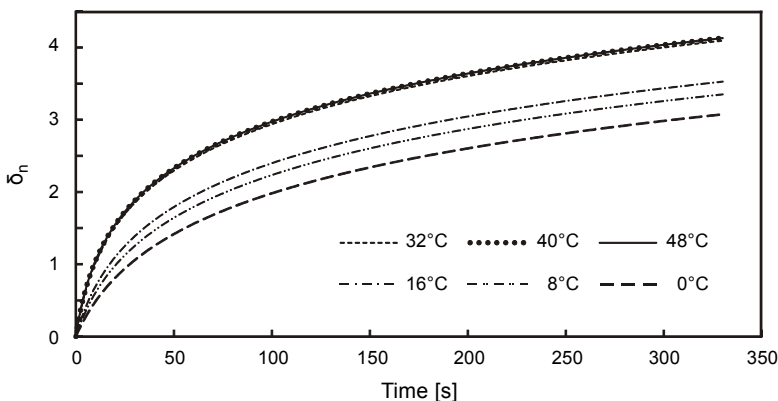
Fig. 8. Normalized approximation waveforms (see the Table).
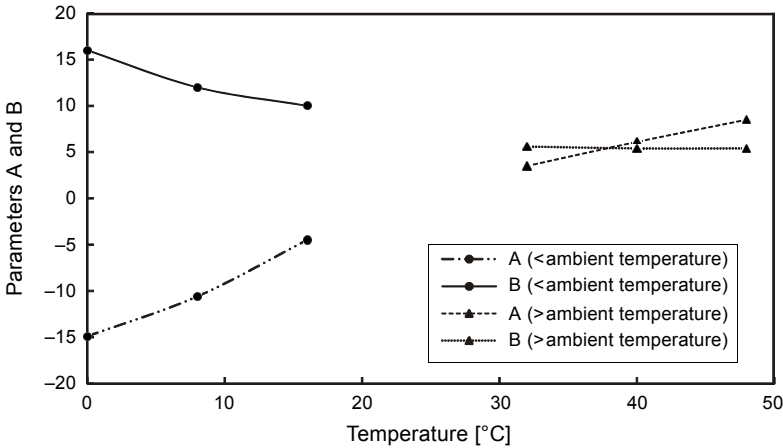
Fig. 9. Dependence of parameters *A* and *B* on exposure temperatures.

smaller in comparison with the waveforms of temperatures higher than the ambient temperature 24°C. As is evident from Fig. 5 and also from sensitivity characteristics, the resulting response is larger for lower temperatures.

Sensitivity characteristics can be expressed by means of the parameters *A* and *B* presented in equations in the Table. For the temperature range of temperatures higher than 24°C, the value of parameter *A* is a basic sensitivity parameter. With respect to almost the same development of normalized waveforms, the value of parameter *B* is constant. The development of parameters *A* and *B* is shown in Fig. 9. This development can be regarded as linear dependence. In fact, the phase shift for these temperatures can be expressed by substituting for *A* the linear approximation equation corresponding to Fig. 9,

$$A = 0.31 v - 6.47 \tag{10}$$

By substituting *A* in (7) we obtain

$$\delta_{ap}(>24°C) \ = \ \pi (0.31 v - 6.47) \ln \left(\frac{t}{5.5} - 1 \right) \tag{11}$$

The temperature dependence of parameters *A* and *B* and the following general phase shift relations can be described in a similar way. The dependence of parameters *A* and *B* on exposure temperature is given in Fig. 9. A general relation for the phase shift is more complicated because of the variability of parameter *B*. On the assumption that the dependence of parameters *A* and *B* will be linearized with respect to temperature, the time dependence of phase can be described by the general equation

$$\delta_{ap} \ = \ \pi (0.65 v - 15.2) \ln \left(\frac{t}{-0.37 v + 15.67} - 1 \right) \tag{12}$$

This equation determines a general dependence, but in view of potential errors or difficult measuring conditions, the above dependence is applicable only to preliminary analysis. It follows from a comparison that for temperatures below 16°C the sensitivity is greater than for temperatures above 32°C.

6. The velocity of phase change

An approximation of the velocity of phase change can be determined from Eq. (5), where ξ is substituted with time t. It is, in fact, the angular velocity of phase change. After modification according to (8), we obtain

$$\left(\frac{d\delta}{dt}\right)_a = \frac{2\pi}{kt + \eta} = \frac{2/k}{t + \eta/k}\pi = \frac{A}{t + B}\pi = \omega_a \tag{13}$$

where the value of π was factored out, identically with the depiction of phase shift curves, as a multiple of π. Curves of angular velocities for individual exposure temperatures are shown in Fig. 10.
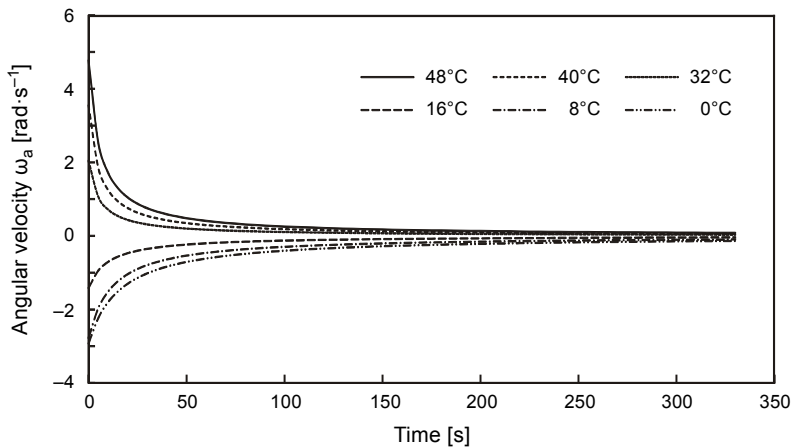
Fig. 10. Course of angular velocity of the phase shift in dependence of the time.

From Fig. 10 the change of the phase shift velocity with time is evident. All curves are calculated in the time interval from 0 to 330 s with a time interval of 5 s. From the data obtained, it is possible to find a direct correspondence with the phase shift curves in Figs. 3 and 4. Worth attention is the earlier mentioned difference in the velocity of phase shift for lover and higher temperatures than ambient, corresponding to the curves of normalized equations depicted in Fig. 6 for angular velocity. The resulting phase shift velocity is for lover temperatures higher due to the higher sensitivity, which is evident from Fig. 9. Monitoring the velocity of phase shift can thus be one of the methods of phase shift evaluation, for example via the number of passages through zero, if the phase shift velocity is known.

7. Discussion

Experimental results prove the possibility of application of the birefringent optical fiber as a sensor element. Shielding the sensor section from the effects of heat transfer by conduction and convection and highlighting the effect of heat transfer via radiation allows reaching defined and reproducible results. In view of the high sensitivity polarization changes owing to assorted parasitic effects it is a significant contribution. It was shown that under given defined conditions the results are not only reproducible but also analytically describable. This allows implementing a system design of sensor arrangement with predictable properties regarding the given parasitic effects. To interpret the polarization of output optical radiation, a polarimeter was used. Measuring the Stokes and other parameters such as the degree of polarization, enables a deeper analysis of the problem than it would be in the case of the simple polarizer and photodetector of the supposed sensor.

Using the polarimeter, on the other hand, affects adversely some results, mainly in the time intervals, where the velocity of phase shifts is very high. The limited sample frequency does not catch exactly the sequence of changes at the high velocities of phase variation, which occur mainly at the start of measurement. Since an analytical description is based on the physical model, whose significance was evaluated by measurement practically in the whole interval of times, it is possible to use this description also for time intervals where the sampling of polarimeter fails.

Of interest is also the linear dependence of fiber response on the exposure temperature, which again predictably describes the sensitivity of fiber. On the other hand, the analysis discovers during the measurement some problems with temperatures lower than ambient. The simple visual examination of curves is complemented with an analysis that allows explaining and subsequently finding some problematic points of the procedure.

In the course of interpreting the phase changes, a combination presents itself of the time response, inclusive of information about the velocity and the resulting phase change, and a set of sensitivity characteristics. This provides a relatively wide range of possibilities in future evaluations of the output signal of sensor.

8. Conclusions

The paper follows up on the previous one [1], where a mechanism of phase change owing to absorbed heat was described in detail. The measuring arrangement allows suppressing the effects caused by thermal conduction and convection, and defining only the effect of thermal radiation. It is about the long-wave region of thermal radiation, with temperatures from 0 to 48°C. Naturally, the range of temperatures can be much wider and with stronger responses from the phase shift point of view. In our work, however, the effect of bodies in the ambient temperature range of 24°C was assumed for potential sensor arrangement.

The results obtained from measurement were analyzed in order to find parameters for the description of the given arrangement. This approach turned out to be real in terms

of the relatively precise description and useful in terms of demand on the expectable behavior of the sensor set.

The possibility of a sufficiently precise description of fiber behavior during thermal exposure also proved the availability of final arrangement, inclusive of the connections of separate parts of fibers, placing the sensor parts and isolation of parasitic effects on the fibers that connect the sensor part with the source of light and the polarimeter.

Further work is expected to be oriented towards specifying the design solution of the final sensor, analyzing the effect of light source, in particular from the viewpoint of spectral parameters, suppression of parasitic effects, *etc*.

References

[1] KYSELAK M., DVORAK F., MASCHKE J., VLCEK C., *Phase response of polarization-maintaining optical fiber to temperature changes*, Optica Applicata 47(4), 2017, pp. 635–649.

[2] KYSELAK M., VLCEK C., MASCHKE J., DVORAK F., *Optical fibers with high birefringence as a sensor element*, Proceedings of 2016 IEEE 6th International Conference on Electronics Information and Emergency Communication (ICEIEC 2016), 2016, pp. 190–193.

[3] DVORAK F., MASCHKE J., VLCEK C., *The response of polarization maintaining fibers upon temperature field disturbance*, Advances in Electrical and Electronic Engineering 12(2), 2014, pp. 168–176.

[4] DVORAK F., MASCHKE J., VLCEK C., *The analysis of fiber sensor of temperature field disturbance by human body part access*, Advances in Electrical and Electronic Engineering 12(6), 2014, pp. 575–581.

[5] DVORAK F., MASCHKE J., VLCEK C., *Utilization of birefringent fiber as sensor of temperature field disturbance*, Radioengineering **18**(4), 2009, pp. 639–643.

[6] SHURCLIFF W., *Polarized Light, Production and Use*, Harvard University Press, Cambridge, London, 1962.

[7] BORN M., WOLF E., *Principles of Optics*, 7th Ed., Cambridge University Press, 1999, pp. 556–570.

[8] FENG ZHANG, LIT J.W.Y., *Temperature and strain sensitivity measurements of high-birefringent polarization-maintaining fibers*, Physics and Computer Science Faculty Publications, 1993, article ID 24.

[9] DOMANSKI A.W., *Polarization degree fading during propagation of partially coherent light through retarder*, Opto-Electronics Review **13**(2), 2005, pp. 171–176.

[10] LESIAK P., *A hybrid highly birefringent fiber optic sensing system for simultaneous strain and temperature measurement*, Photonics Letters of Poland **2**(3), 2004, pp. 140–142.

[11] SANG MIN JEON, YONG PYUNG KIM, *Temperature measurements using fiber optic polarization interferometer*, Optics and Laser Technology 36(3), 2004, pp. 181–185.

[12] COLLETT E., *Polarized Light in Fiber Optics*, Lincroft, New Jersey, USA, 2003.